Journal of Soils and Sediments
https://doi.org/10.1007/s11368-017-1878-y

SOILS, SEC 5 • SOIL AND LANDSCAPE ECOLOGY • RESEARCH ARTICLE

A laboratory study on rill network development and morphological characteristics on loessial hillslope

Chao Qin[1,2] • Fenli Zheng[1,3] • Ximeng Xu[1,2] • Hongyan Wu[1] • Haiou Shen[4]

Received: 3 June 2017 / Accepted: 19 November 2017

Abstract

Purpose Rills are basic pathways for runoff, sediment, and pollutant transport at hillslopes within agricultural watershed. The objectives of this study were to investigate the development processes of rill network and morphological characteristics and to examine their affecting factors.

Materials and methods A soil box (10 m long, 1.5 m wide, and 0.5 m deep) was subjected to four successive simulated rains under rainfall intensity of 90 mm h^{-1} with slope gradients of 15° and 25°. Digital elevation models (5 mm resolution) were created from the terrestrial laser scanning measurements.

Results and discussion Total soil loss was 46.3 and 61.0 kg m^{-2} at the 15° and 25° slope gradients, and rill erosion occupied over 75% of the total soil loss. Soil loss and rill erosion were expressed as power equations to the product of slope gradient and accumulated rainfall. Rill networks evolved in a converging way and reached maturity in the fourth rain. Main rill length and rill width, depth, and degree of contour line departure increased with increased rains, while rill width/depth ratio showed the opposite trend. Secondary rill length and rill density increased in the first two rains, and then both decreased in the latter two rains. Scour effect of lateral interfluve flow and meander cutoffs of rill flow were two sub-processes of rill piracy. Rill length and density decreased due to rill piracy specific in merging of secondary rills into main rills. Plow pan and secondary headcuts played key roles in main rill bed incision and sidewall expansion processes, while both had little impact on secondary rills.

Conclusions Results of this study can improve the understanding of how plow pan, rill piracy, and secondary headcut affect rill network and morphologies and provide fundamental knowledge for designing rill prevention practices.

Keywords Plow pan · Rill morphology · Secondary headcut · Soil erosion · TLS

1 Introduction

Soil erosion is a widespread problem for sloping croplands and represents a severe environmental issue on the Loess Plateau of China. Rills occur on smooth side slopes above drainage ways, which are defined as small, intermittent water courses that present no obstacles to tillage using conventional equipment (Lal 2002). Its width and depth usually varies between 3 to 30 and 3 to 20 cm, respectively (Zhu 1956; Foster et al. 1983). Rill erosion, one of the dominant erosion processes on hillslope, is often triggered by high-intensity and short-duration rainstorms (Foster et al. 1983; Zhou and Wang 1987; Mancilla et al. 2005). It accounts for approximately 70% of soil loss on rill-dominated loessial hillslopes (Zhu 1956). Within the continuum of soil erosion growth stages, rills are important erosional landforms of hillslopes through which runoff, sediment, and nutrients can be transported into gullies. Once rills appear on the hillslope, concentrated flow in rills has greater hydraulic erosive force and higher transport capacity than sheet flow. So it is important to understand the formation of rills and key factors that contribute to rill development processes.

Responsible editor: Renduo Zhang

✉ Fenli Zheng
flzh@ms.iswc.ac.cn

1 Institute of Soil and Water Conservation, State Key Laboratory of Soil Erosion and Dryland Farming on the Loess Plateau, Northwest A & F University, Yangling 712100, Shaanxi, People's Republic of China

2 National Center for Computational Hydroscience and Engineering, University of Mississippi, Oxford, MS 38677, USA

3 Institute of Soil and Water Conservation, CAS & MWR, Yangling 712100, Shaanxi, People's Republic of China

4 Collage of Resources and Environment, Jilin Agriculture University, Changchun, 130118 Jilin, People's Republic of China

Published online: 12 December 2017

Rill network develops through the processes of rill bifurcation, merging, and connectivity (Brunton and Bryan 2000; Mancilla et al. 2005; Berger et al. 2010). Berger et al. (2010) indicates that rill networks often develop in complex ways, and their development processes vary according to the soil conditions. Other studies have found that slope length, gradient, and soil surface roughness play key roles in determining the degree of complexity in rill networks (Horton 1945; Mancilla et al. 2005). Brunton and Bryan (2000) conducted series of simulated rainfall experiments and indicated that rill network development started with initial knickpoint incision and subsequent network evolution was controlled by headward migration of knickpoints and incision of the main channel. On the other hand, rill morphology has evident effects on rill erosion and rill network development (Govindaraju and Kavvas 1994). Rill morphology determines flow convergence or divergence; it also contributes to the uncertainty and complexity of three main processes of rill development (rill head advance, rill bed incision, and rill sidewall expansion) which cause a non-uniform distribution of rill spacing and efficiency (Bingner et al. 2016). Studies concerning headward retreat, bed incision, and sidewall expansion have provided the theoretical basis for comprehensively researching rill network evolvement and response of rill morphology to hydrological process and topographic characteristics (Bryan and Poesen 1989; Bennett et al. 2000; Mancilla et al. 2005; Wells et al. 2013). However, current studies mainly focused on rill network formation and development on gentle slopes, quantifications of rill networks and corresponding morphological characteristics on steep slopes especially on the Loess Plateau of China, are not well described. Several factors and processes such as secondary headcut, plow pan, and rill piracy greatly impact rill morphology and rill network development.

The occurrence and migration of headcuts play a critical role in rill formation and drainage system evolution (Bryan and Poesen 1989; Bennett et al. 2000). Initial drop-pits, which develop at smooth slope surface and caused by surface seal failure, facilitate the formation of rills, while secondary headcuts, which develop only in well-established rills, determine bed roughness to a great extent (Bryan and Poesen 1989). It is essential to make clear how rill depth change with time with and without secondary headcuts, but, currently, there are few studies focused on the rill bed incision process before a headcut arrived and after another former headcut moved forward.

Rill piracy and competition, where one rill erodes headward to capture the drainage of another rill, have great impact on rill network and morphology development (Favis-Mortlock et al. 2000). Based on the ability to competing for runoff, rills have been divided into two types: successful rills and unsuccessful rills (Favis-Mortlock et al. 2000). Berger et al. (2010) indicated that rill piracy appeared more often, and more intensive rill incision occurred under higher rainfall intensity and slope. Thus, more attention should be paid to the rill development process under the role of high-intensity erosive rainfall and steep slope gradient.

Plow pan, which has a resistance to erosion greater than that of the overlying soil, often develops due to conventional tillage operations (Wells et al. 2013). Significant changes occurred among the processes of headward advance, bed incision, and sidewall expansion when plow pan exposed to concentrated flow (Fullen 1985; Gordon et al. 2007; Wells et al. 2010; Wells et al. 2013; Shen et al. 2015). However, detailed research on changes in rill morphology when plow pan occurred based on high-resolution DEMs still needs to be intensified.

Many studies have been done to monitor rill and rill network development. However, few studies have focused on the comprehensive evaluation of the effects of rill piracy, secondary headcut, and plow pan on rill morphologies on steep loessial hillslopes. Researches on this topic may attribute to further understanding of rill erosion and provide fundamental knowledge for designing rill prevention practices. Therefore, a series of laboratory experiments were conducted to investigate the development of rill networks and morphology. The specific objectives were as follows: (1) to quantify the temporal variations of rill network and morphology by using morphological indicators extracted from high-resolution DEMs obtained by terrestrial laser scanning technique and (2) to quantify how rill piracy, plow pan, and secondary headcuts affect rill network and morphology development with time.

2 Materials and methods

2.1 Experimental materials

The study was conducted at the State Key Laboratory of Soil Erosion and Dryland Farming on the Loess Plateau in Yangling City, China. A down pointing rainfall simulator system was used to apply rainfall. The rainfall simulator, which includes three sets of nozzles, can be set to any selected rainfall intensity ranging from 30 to 350 mm h^{-1} by adjusting the nozzle size and water pressure. The raindrops fall from 18 m above the soil surface, which allow > 90% raindrops to reach terminal velocity prior to hitting the soil surface. The simulated rainfall was similar to natural rainfall regarding the raindrop size distribution, kinetic energy, and uniformity (> 90% for 20° slope gradient) (Zhou et al. 2000). A soil box with 10.0 m long, 1.5 m wide, and 0.5 m deep, which has a proper size for runoff generation, headcut advance, and network development, was used in this study (He et al. 2014; Shen et al. 2015). Similar to Momm et al. (2016) and Wells et al. (2016), drainage holes (2 cm grid spacing) at the soil box bottom were to use for drainage. The soil box can be inclined in 0.5°

adjustment steps to achieve a slope gradient from 0 to 30°. A runoff collecting device was installed on the outlet of the soil box to collect runoff samples throughout the rainfall.

The soil used in this study was loess (geological deposits, fine-silty, and mixed), which can be classified as a *Calcic Cambisol* (USDA NRCS 1999). The top 20 cm of the Ap horizon was collected at a well-drained site in Ansai Town (36°45′ N, 109°11′ E), which is typical of the hilly region of the Loess Plateau of China (Yang et al. 2006; Shen et al. 2015). The soil texture was 28.3% sand (> 50 μm), 58.1% silt (50–2 μm), 13.6% clay (< 2 μm), and contained 5.9 g kg^{-1} soil organic matter, and the pH in water was 7.95. The soil was not recycled from previous experimental runs. Impurities such as organic matter and gravels were removed from the soil, though to keep its natural state, the soil was not passed through a sieve (Shen et al. 2015).

2.2 Experimental setup and procedure

To form well developed rill networks, successive simulated rains were applied (Wells et al. 2016). In this study, four series of rains (two replicates with two slope gradients, each series contained four successive rains) were applied. Because the area with slope gradient ranges between 14° and 28° accounts for more than 75% of loess interfluve (Zhou and Wang 1987), and rills frequently develop on the loessial hillslopes with slope gradient > 15°, 15° and 25° slope gradients were used in this experiment. According to the observed natural erosive rainstorms that may cause intensive rill erosion (maximum 5 min rainfall intensity was 1.52 mm min^{-1}, I_5 = 1.52 mm min^{-1}; maximum 15 min rainfall intensity was 1.44 mm min^{-1}, I_{15} = 1.44 mm min^{-1}; maximum 30 min rainfall intensity was 1.18 mm min^{-1}, I_{30} = 1.18 mm min^{-1}), the designed rainfall intensity for each 20-min rain in this study was set to 1.5 mm min^{-1} (Zhou and Wang 1987). According to the durations of natural erosive rainstorms (vary from 5 to 600 min) on the Loess Plateau, and among which 40–70% lasts less than 1 h (Zhang 1983), the total rainfall duration was set to 80 min, including four 20-min successive rains (i.e., first rain, second rain, third rain and fourth rain). According to the former researches (He et al., 2014; Shen et al., 2015) and the observed data on the sloping cropland, bulk density of plow pan and plow layer in this research were designed as 1.35 and 1.10 kg m^{-3}, respectively. To acquire high-resolution DEMs during different phases of rill development, terrestrial laser scanning measurements (TLS) were conducted to determine changes in the soil surface before run and after each successive rain. The interval between each rain was about 5 min (not included in each 20-min successive rainfall), which was long enough to minimize the water redistribution effect and to apply the scanning procedure. Specifically, the laser scanner was mounted on a triangular shelf bracket 4.5 m above the ground and 2.0 m in front of the soil box. The purpose of mounting the scanner in a high position relative to the soil box instead of applying multiple scans is to save time and reduce the shadowing of the irregular rill sidewalls so that accurate point clouds and high-resolution DEMs may be possibly obtained. Figure 1a shows the point clouds after filtering redundancies without evident points missing.

2.2.1 Preparation of the soil box

Before packing the soil box, the soil water content (usually ranges 11–13%) was determined and used to calculate how much soil was needed for packing. The soil box was filled from the bottom to the top with sand and soil material. An 80 × 80-cm iron plate with a handle, weighed 5 kg, was used to pack each layer manually. Firstly, the lower 10 cm of the soil box was filled with sand to allow free drainage of excess water. A highly permeable cloth was used to separate the sand and soil layers. Secondly, a 10-cm plow pan with a soil bulk density of 1.35 g cm^{-3} was packed above the sand layer. Thirdly, a 20-cm tilled layer with a soil bulk density of 1.10 g cm^{-3} was packed above the plow pan, each in 5-cm increments (Shen et al. 2015; Momm et al. 2016). The whole packing duration was limited to less than 3 h to minimize the soil recovery during the packing. Then, the soil box was allowed to settle for 48 h.

2.2.2 Experimental procedure

Before conducting each experiment, pre-rain was applied at an intensity of 30 mm h^{-1} for approximately 30 min using a slope gradient of 3° until surface runoff occurred (Momm et al. 2016; Wells et al. 2016). The purpose of the pre-rain was to maintain consistent soil moisture, consolidate loose soil particles by raindrop compaction, and reduce the spatial variability of underlying soil conditions. The average soil water content before the first rain was 23.0 ± 0.5% for all treatments. A plastic sheet was used to cover the soil box surface to prevent evaporation during 24 h of soil box settling. Then, the rainfall intensity was calibrated for the target rainfall intensity (90 mm h^{-1}). For each rain, after runoff occurred, runoff samples were collected and weighed in 20-l buckets in 1–2 min intervals for the whole rainfall durations. Flow velocity (including velocities of rill, inter-rill and lateral interfluve flow, which refers to inter-rill flow captured by rill) was measured using the dye tracing method, and in which $KMnO_4$ solution was used as a dye (Giménez and Govers 2001). Then, flow velocity was calculated by recording the travel time of the dyed runoff over a certain distance. Travel time was taken as the mean of three measurements. Value of measured flow velocity was then used to estimate the mean flow velocity by timing a coefficient *k* (0.67 for laminar flow, 0.7 for transitional flow, and 0.8 for turbulent flow) (Li et al. 1996). After

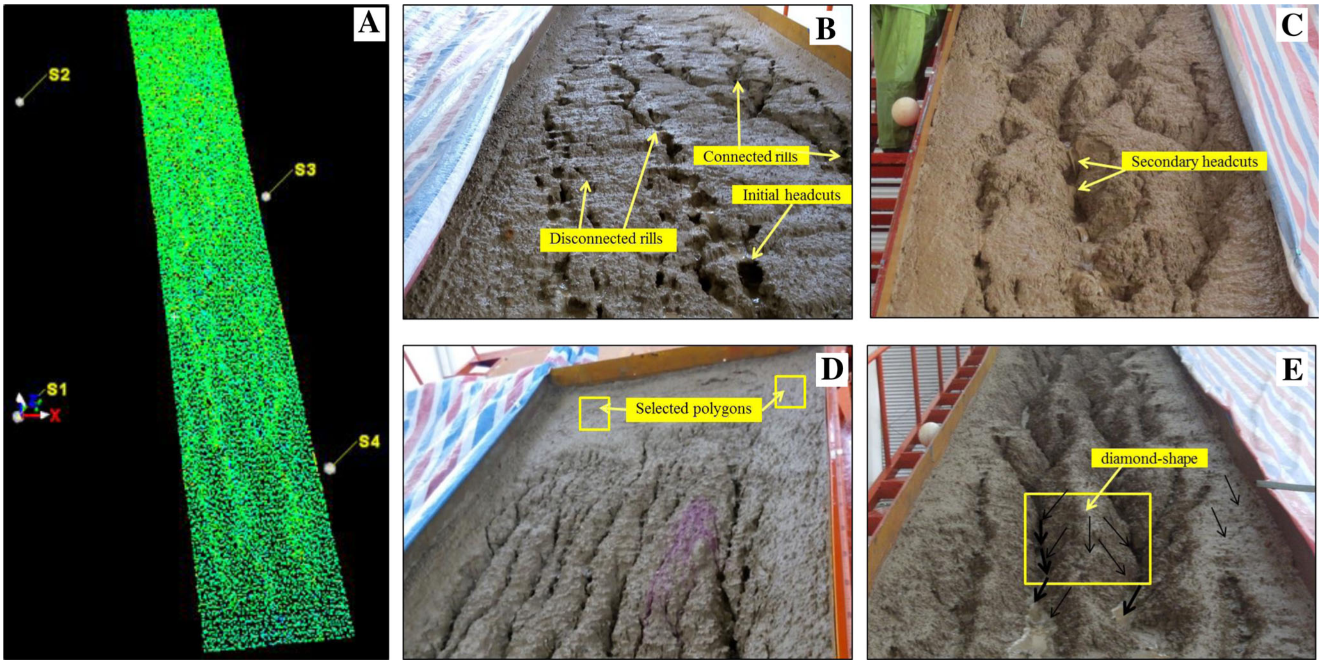

Fig. 1 **a** Point cloud data after filtering redundancies. **b** Initial headcut, disconnected, and connected rills at the first rain. **c** Secondary headcuts in the main rills. **d** Small and narrow secondary rills at the upper part of the soil box. **e** Deep and wide main rills at the lower part of the soil box. Arrows in different weight in **e** represent flows of rill (widest), inter-rill (middle width), and lateral interfluve (finest). S1, S2, S3, and S4 in **a** represent four targets

rainfall, runoff samples were left over night to settle so that the excess water could be decanted. The samples were then dried in an oven at 105 °C for 24 h and weighed to calculate runoff and total soil loss.

2.3 Terrestrial laser scanning equipment and evaluation

A Leica Scanstation 2, Terrestrial Laser Scanner (Leica Geosystems Inc., Switzerland) was used to measure changes in the hillslope surface. Images and point clouds (with minimum resolution of 4 mm × 4 mm at the maximum distance away from the scanner) were acquired by the scanner to quantify surface changes. Overall, 107.3 thousand points were obtained for each rain in the following analysis (Cyclone 6.0 software, Leica Geosystems Inc., Switzerland). A series of preprocessing operations (including denoising, coordinate transformation and down sampling) were accomplished. The aim of down sampling was to alleviate the impacts of different point cloud densities in the process of generating DEMs and speed up the calculation process. After preprocessing, point clouds (approximately 5.6 thousand points) were exported with the .txt format and then imported into ArcGIS 10.0 to construct DEMs. The nearest neighbor interpolation method was used to calculate a grid of values from data that can be a combination of regular, sparse, clustered, or random distributions of points (Vinci et al. 2015). The resolution of DEM was averaged to 5 mm × 5 mm raster grids, and based on the high resolution DEMs, the following analysis was implemented. According to the definition of rill given by Zhu (1956) and Foster et al. (1983), a relative elevation of 1 cm was set as the criteria to identify rill areas and inter-rill areas. Flow accumulation threshold was set as 150, which can ensure enough upstream drainage area to produce rills with their depths > 1 cm. Drainage extraction was applied using Spatial Analyst function and ArcHydro tool. The detailed operating steps included calculating aspect, flow direction, flow accumulation and stream definition, stream segmentation, and drainage line processing.

The volume difference between two DEMs could be attributed to soil material self-settling, raindrop compaction, splash, sheet, and rill erosion. To separate rill erosion from other factors that cause the volume difference between two DEMs, supplementary measurements were applied. Elevation difference of the area without rill development at the 0–1 m slope length was calculated by confining two 30 cm × 30 cm polygons (Fig. 1d). With the assumption that self-settling, raindrop, and sheet erosion led to the same amount of volume difference between selected polygons and the rest of the soil box, the volume difference caused by rill erosion might be expressed as follows:

$$\Delta V_{rill} = \Delta V_{total} - \Delta H/0.09 \times 1.5 \times 10 \times \rho \quad (1)$$

where $\triangle V_{rill}$ is volume difference caused by rill erosion (m^3), $\triangle V_{total}$ is total volume difference between two DEMs (m^3), $\triangle H$ is mean elevation difference of the two selected polygons (m), ρ is soil bulk density (kg m^{-3}), 0.09 is average area of the selected polygons (m^2), and 1.5 and 10 are width and length of the soil box, respectively (m). Then, rill erosion was calculated by volume differences of two DEMs (before and after each rain), elevation differences of selected polygons, and given soil bulk density.

European stream order classification theory proposed by Gravelius (1914) was used to identify the rill network classification. The whole process was fulfilled manually with seven steps: (1) rill network generation; (2) rill length calculation; (3) rill width measurement at every 10-cm interval; (4) defining the longest, widest, most branched, or stem single channels as main rills (order 1); (5) defining the channels directly contributed to the order-1 rills as the secondary rills (order 2); (6) defining the channels contributed to the secondary rills as the third-order rills and so on (Fig. 2 (B-15°)); and (7) for rills that were not connected, main rills were defined as the longest and largest channels in the same flow path (order 1). Secondary rills were the branched channels of the main rill (order 2, 3, 4….) (Fig. 2 (A-15°)).

2.4 Indicators for describing rill network development and morphology

2.4.1 Rill density

Rill density (d) has been used as a morphological indicator of water erosion and rill network development and is a measure of how well a contributing area (CA) is drained by rills (Bewket and Sterk 2003). Rill density reflects the degree of hillslope fragmentation, and higher d values indicate greater soil erosion rates and higher bifurcation ratios (Shen et al. 2015). The value of d is calculated for a given unit slope length (from the top edge of soil box) as follows:

$$d = \sum_{i=1}^{n} L_i / A \tag{2}$$

where d is rill density (m m^{-2}), L_i is the total length of the ith rill segment and its bifurcations (m), A is the area of the CA or sub-unit (m^2), and $i = 1, 2, \ldots, n$ represents the number of measurement points.

2.4.2 Degree of contour line departure

The degree of contour line departure (μ) is defined as the ratio of the change in contour line length to the original contour line length. A higher μ value indicates a more developed rill network and a more fragmented hillslope surface morphology. It can comprehensively reflect the development degree of rill network and their morphological characteristic. The value of μ is calculated as follows:

$$\mu = \left(L' - L\right) / L \times 100\% \tag{3}$$

where μ is the degree of contour line departure (%), L is the original contour line length (m), and L' is the contour line length after rain (m).

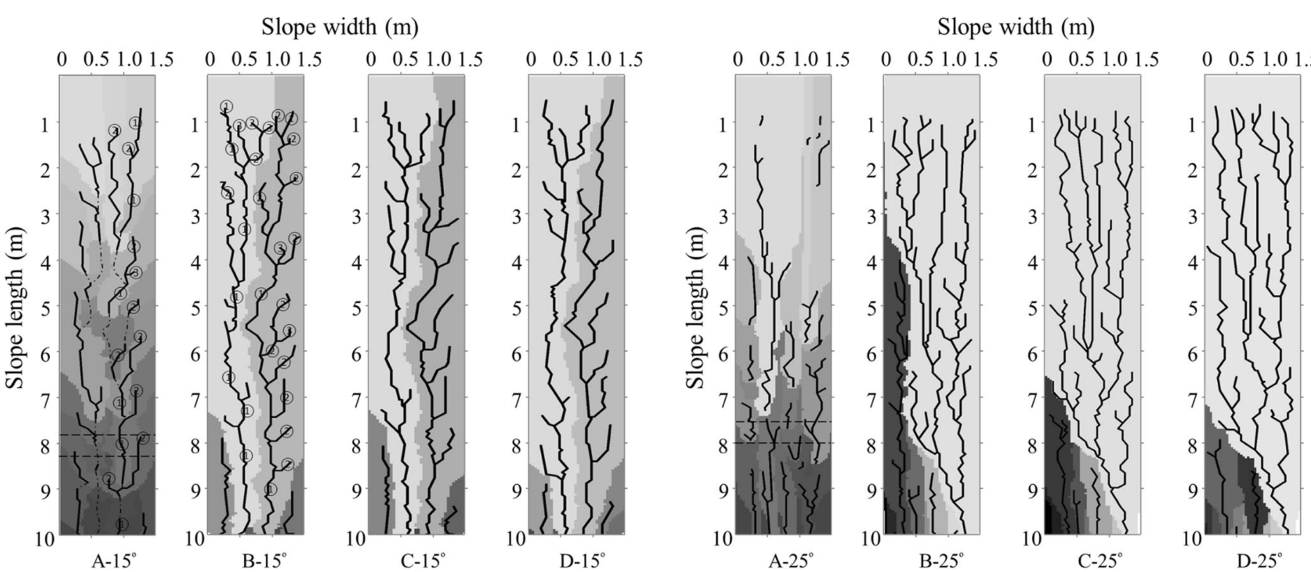

Fig. 2 Rill network delineation after the first (A-15°, A-25°), second (B-15°, B-25°), third (C-15°, C-25°), and fourth (D-15°, D-25°) rains with slope gradients of 15° and 25°. Numbers and dashed dot lines in A-15° and B-15° represent rills in different orders and potential rills that in the same flow paths, respectively. Area between two horizontal dashed lines in A-15° and A-25° represents initial rill head occurrence position

3 Results and discussion

3.1 Runoff and soil loss

Runoff rate increased from the first rain to the fourth rain for both slope gradients and was significantly lower in the first rain than those in other rains (Table 1). It accounted for 55.3 to 94.0% of the target rainfall intensity (1.5 mm min^{-1}) and confirmed the status of over seepage flow (Wu et al. 2014). Soil loss increased first and then decreased for both treatments. It decreased in the fourth rain while runoff increased, which could be attributed to a decrease in sediment concentration (Table 1).

Unlike total soil loss, rill erosion gradually increased from the first to fourth rain (Table 1). Rill erosion only accounted for less than 60% of total soil loss for the first rain while it occupied more than 70% of total soil loss as rills became connected in the second, third, and fourth rains, which confirms the key process of rill erosion on hillslope. Rill erosion reached relatively stable stage at the third rain for the 15° slope gradient while at the second rain for the 25° slope gradient, which implies the increase of slope gradient, it can facilitate the rill development process. Contribution of rill erosion to total soil loss in this study corroborates that obtained by Zheng and Tang (1997) and Zhu (1956) in both field and laboratory scale, who noted that rill erosion accounted for about 70% of total soil loss.

Soil loss has been shown to be related to the slope gradient and contributing area in steep slope conditions (Liu et al. 1994; Gong et al. 2011). Regression analysis showed that soil loss and rill erosion had significant power correlation with the product of slope gradient and accumulated rainfall. The soil loss and rill erosion can be expressed as follows:

$$SL = 8.843(RS)^{1.529} \quad \left(R^2 = 0.965, P < 0.05, n = 24\right) \tag{4}$$

$$E_{rill} = 5.265(RS)^{1.717} \quad \left(R^2 = 0.950, P < 0.05, n = 24\right) \tag{5}$$

where SL is accumulated soil loss, E_{rill} is accumulated rill erosion, R is accumulated rainfall, and S is slope gradient. The exponents of soil loss and rill erosion were 1.529 and 1.717, respectively, which indicated that the effect of rainfall and slope on rill erosion was higher than that on total soil loss.

3.2 Rill network development processes

Generally, rill networks evolved through an initial phase of increasing complexity as secondary tertiary rills converged into main rills and followed by a phase of stable rill network (Fig. 2). A large number of rills formed during the first rain and inter-connected during the second rain for both treatments (Figs. 1b, 2 (A-15°, A-25°, B-15°, B-25°)). Initial rill head occurrence positions were 7.8 to 8.3 and 7.5 to 8.0 m slope lengths at the 15° and 25° slope gradients, respectively (Fig. 2 (A-15°, A-25°)), which confirmed that rill initiation was hydraulically controlled and conformed with established threshold conditions (Bryan and Posen 1989; Gordon et al. 2007). Soil intrinsic properties, e.g., soil erodibility and critical shear stress, are other factors that would affect potential headcuts occurrence place (Gordon et al. 2007). Similar results were obtained by Brunton and Bryan (2000), who indicated that the occurrence position of initial headcuts move upslope with the increase of slope gradient. The average distance between two initial rill headcuts at the 15° slope gradient was 23.9 cm, and it was 2.9 cm longer than that at the 25° slope gradient. The regular spacing between two headcuts was likely attributed to flow hydraulic properties, flow roll waves, and shear stress (Bryan and Posen 1989). At the second rain, initial rill network had been formed and rill erosion intensified through the processes of rill bifurcation, connectivity, and merging (Fig. 2

Table 1 Runoff, soil loss, and rill erosion for the four successive rains

Slope gradient (°)	Successive rains	Runoff rate (mm min^{-1})			Soil loss (kg m^{-2})			Rill erosion (kg m^{-2})			Contribution of rill erosion to soil loss (%)		
		1	2	Avg	1	2	Avg	1	2	Avg	1	2	Avg
15	1st	0.87	0.79	0.83a	3.88	4.62	4.25a	2.12	2.78	2.45a	54.7	60.3	57.5
	2nd	1.27	1.21	1.24b	10.19	11.28	10.73b	7.11	8.17	7.64b	69.8	72.5	71.2
	3rd	1.40	1.35	1.38b	15.95	16.82	16.39c	12.06	12.80	12.43c	75.6	76.1	75.9
	4th	1.41	1.37	1.39b	14.02	15.80	14.91c	11.64	13.37	12.50c	83.0	84.6	83.8
25	1st	0.90	0.85	0.88a	8.03	7.21	7.62a	4.16	3.65	3.90a	51.8	50.6	51.2
	2nd	1.28	1.24	1.26b	20.08	18.05	19.07b	14.76	13.00	13.88b	73.5	72.0	72.8
	3rd	1.37	1.41	1.39b	18.26	17.12	17.69b	14.46	13.47	13.97b	79.2	78.7	79.0
	4th	1.38	1.44	1.41b	17.05	16.11	16.58b	14.68	13.66	14.17b	86.1	84.8	85.5

Note: Average values under the same slope gradient followed by an identical letter (a, b, or c) in the same column are not significantly different at $P < 0.05$ according to the LSD test

(B-15°, B-25°)). Rill lengthened fast (Fig. 3a) and rill heads advanced to nearly the top of the soil box (0.5–0.9 m slop length; Fig. 1d). Average distance between two headcuts almost maintained stable. The headcut advancing rates were calculated by dividing the increment of total rill length by rainfall duration (20 min). They were 55.4 and 80.6 cm min^{-1} at the 15° and 25° slope gradients, respectively, and were 40.2 and 44.9% smaller than those at the first rain. At the third rain, rill network further developed (Fig. 2 (C-15°, C-25°)). A mature rill network was formed (Fig. 2 (D-15°, D-25°)) by the fourth rain in which the entire slope was dominated by one to two large, well-developed main rill catchment areas (CAs) and some small rill CAs which were located very close to the outlet of the soil box. The headcut advancing rates significantly decreased at the third rain and were nearly zero at the fourth rain.

The CA shape, number, and size changed with rainfall duration (Fig. 2). Due to the discontinuity of small rills in the first rain, there were many independent micro-CAs and some of them were not connected to the outlet of the soil box. The total number of rills was higher than most of the following rains. This was because flow paths were not clear and few bifurcations and connectivities were found (Fig. 2 (A-15°, A-25°)). At the second rain, rill network systems developed and some small CAs were taken over by the main rill CAs (Fig. 2 (B-15°, B-25°)). As a result, the first-order rill number decreased and some third-order rills formed. Rill network system reached the most developed extent among the four rains (Table 2). For the third and fourth rains, the number of the rills in different rill orders kept stable, but there existed rill piracy between the main rill and secondary rills (Fig. 2 (C-25°)).

3.3 Rill morphological characteristics

3.3.1 Rill length, width, depth width/depth ratio, and cross-section analyses

In general, total rill length increased with the increase of rains but main rills and secondary rills demonstrated different trends (Fig. 3a). Through rill head advancing and the connection of a few rills on the same concentrated flow path (Shen et al. 2015), total rill length sharply increased during the first and second rain, while length changes of the main rills and secondary rills showed contrary tendency for the third and fourth rains. This could be explained by the principle of minimization of energy dissipation (Berger et al. 2010; Hofer et al. 2012). As rainfall continues, runoff energy of the entire network dissipated through the processes of rill piracy and competition to keep the system stable. Length of main rills

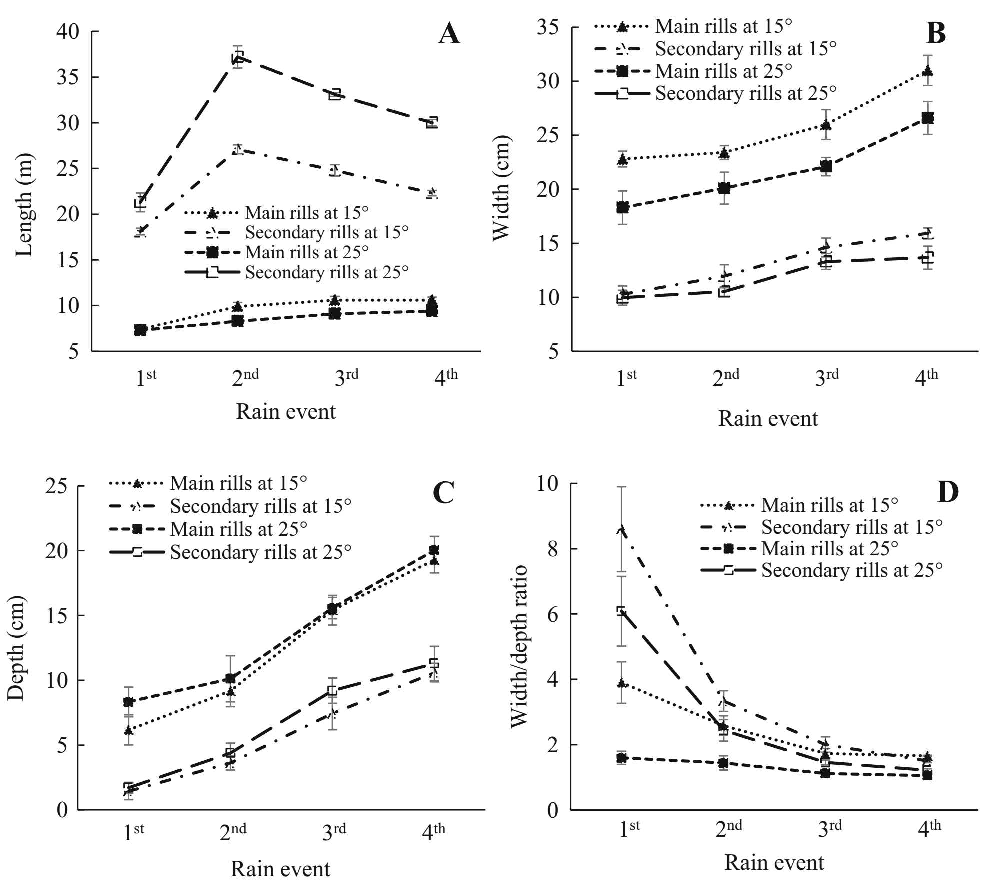

Fig. 3 Average values of two replicates for **a** total length, **b** average width, **c** average depth, and **d** average width/depth ratio of main rills and secondary rills after the first, second, third, and fourth rains with slope gradients of 15° and 25°. Error bars represent the difference between two replicates

Table 2 Number of rills in each order and total rill number for the four successive rains

Slope gradient (°)	Successive rains	Rill order			Total
		1st	2nd	3rd	
15	1st	15	15	1	31
	2nd	4	18	4	26
	3rd	4	14	0	18
	4th	4	12	1	17
25	1st	11	15	2	28
	2nd	4	16	9	29
	3rd	4	8	9	21
	4th	4	5	10	19

developed at the 15° slope gradient was longer than that at the 25° slope gradient while the length of secondary rills was longer at the 25° slope gradient.

The changes of rill length were also affected by changes of rill width and depth. For example, main rill width increases led to the number of secondary rills decreasing which facilitates the total rill length decreases. Unlike the rill length trend, both the main rill width and secondary rill width increased with the increase of rains for both treatments (Fig. 3b). As can be seen from Fig. 3c, rill depth showed the same increasing trend as rill width for all rains.

Both main rill and secondary rill width/depth ratios showed a decrease trend with an increase in rain (Fig. 3d). Though rill width increased with each rain event, the decreasing trend of width/depth ratio indicated that the rate of rill depth increase was faster than that of rill width. Rill cross sections showed different shapes before and after rill bed reaching plow pan. It changed from wide U-shape (first and 2rd rains) to U-shape (third rain) to lagena-shape (fourth rain) (Fig. 4). Rill shoulder occurred at the third rain and became wider at the fourth rain. The remaining area acted as diamond shape at the end of the experiment (Fig. 1e). Rill cross sections obtained in this study were similar to the results given by Fullen (1985) when the effects of plow pan on rill erosion process were firstly studied in the field.

3.3.2 Rill density

Rill density overall decreased in the order of the second, third, fourth, and first rain for both treatments, where the first rain illustrated the largest increase rate (Fig. 5). This result corresponds with the results of Gessesse et al. (2010), who noted that rill density increased during the initial periods and then decreased and fluctuated during the later periods of rainfall processes. The spatial variations of d fluctuated more than the line μ and showed the opposite trend compared with μ (Fig. 5). During four successive rains, d increased to a peak at

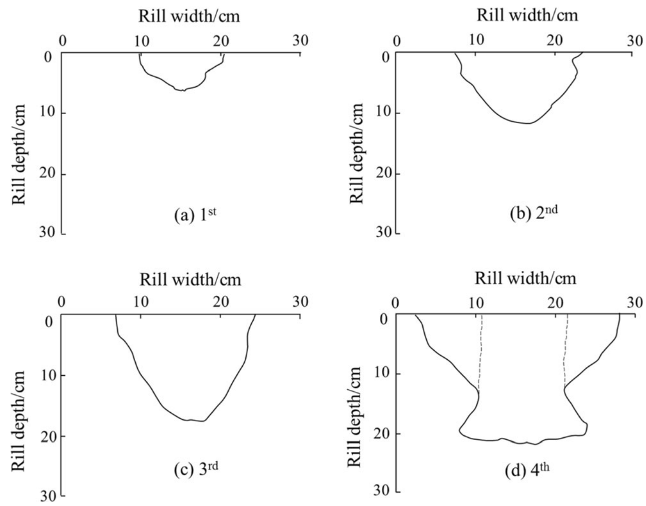

Fig. 4 Sketch of main rill cross sections after **a** the first, **b** second, **c** third, and **d** fourth rains (selected example from one cross section at the slope length of 7.5 m with slope gradient of 15°). The dashed lines show the shoulder developed on the top of the plow pan

a slope length of 2 m and then fluctuated and decreased to comparatively low levels at slope lengths of 3–10 m. This could be attributed to a large number of shallow-narrow small rills developed at the upper part of soil bed (Fig. 1d). A similar principle of rill distribution along the loessial hillslope was illustrated by Shen et al. (2015) and Zheng and Tang (1997).

3.3.3 Degree of contour line departure

The length and curvature of the contour lines increased with rill development during the four successive rains for both slope treatments (Fig. 6). Rill headcuts and disconnected rills occurred during the first rain at a slope length from 7.5 to 9.0 m (Fig. 6 (B-15°, B-25°)). The hillslope surface morphology became incised into fragmented patches, and rill sidewalls could be easily observed such that contour lines deviated from perpendicular to slope during the second rain (Fig. 6 (C-15°, C-25°)). More intensive and tortuous contour lines shown in Fig. 6 (D-15°, D-25°) of the third rain indicates severe undercutting and sidewall expansion. During the fourth rain, the fundamental hillslope surface morphology and micro-CAs did not change significantly but more contour line segments were perpendicular to the horizontal direction (Fig. 6 (E-15°, E-25°)).

For both slope treatments, contour line departure (μ) increased with the increase of rains, and their trend lines fluctuated less and reached maximum values at 7–9 m slope length (Fig. 5). The hillslope was occupied by a large number of short, small, and narrow rills on the upper slope (Fig. 1d) and dominated by deeper and wider rills on the middle and toe slope (Fig. 1e). Similar results were found by Hofer et al. (2012). For the 25° slope gradient, trend lines of μ fluctuated more and reached their maximum 1 m ahead compared with

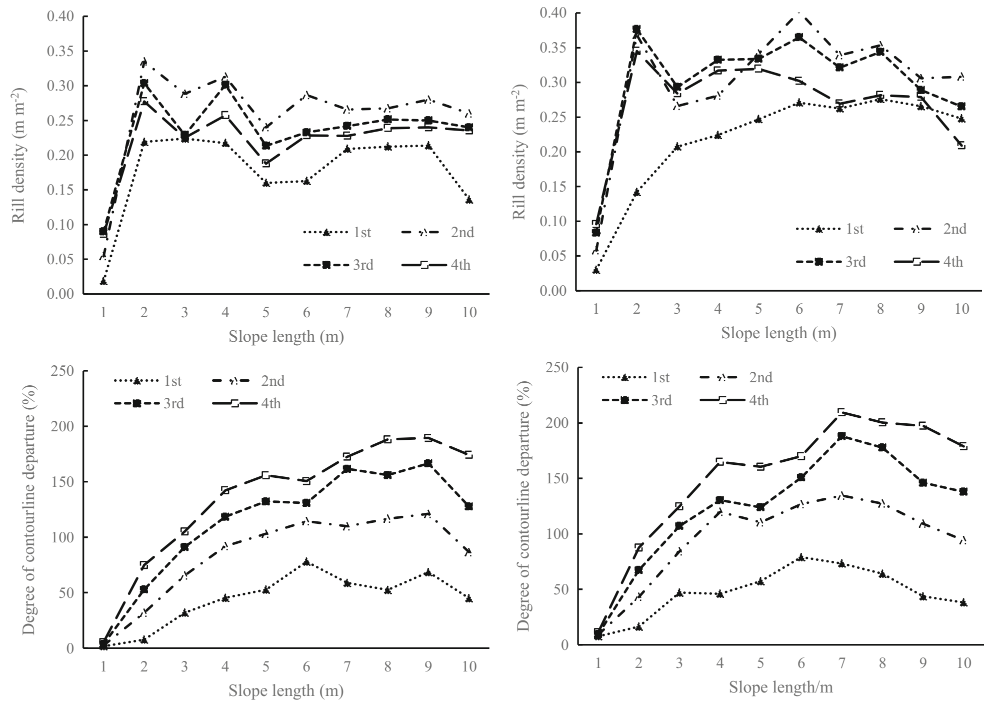

Fig. 5 The rill density (d) and degree of contour line departure (μ) along the hillslope after the first, second, third, and fourth rains with slope gradients of 15° and 25°

those at the 15° slope gradient, which indicated more fragmented hillslope surface at large slope gradient.

3.4 Impacting factors on rill morphology

3.4.1 Rill piracy

Rills on hillslopes often evolve in a converging manner that is similar to the evolution of river networks described by Horton (1945). When rill head completed retreating after the second rain, the dominant erosion process gradually changed into rill widening and deepening. Rill sidewall collapse at the very boundary of CAs may resulted in small CAs taken over by the main rill CAs (Fig. 2 (B-15°, B-25°)). Rill piracy occurred and could be treated as a lateral erosion process (Fig. 2 (C-25°)). Flow velocities of rill, inter-rill, and lateral interfluve (inter-rill flow captured by rills; Fig. 1e) were measured during rain and are shown in Table 3. Inter-rill flow velocity decreased, while both rill and lateral interfluve flow velocities increased with the increase of rains. Two sub-processes contributed to rill piracy: (1) scour effect of lateral interfluve flow on featheredging rill sidewall (soil particles of rill sidewall entrained by inter-rill flow captured by rill flow) enhanced with the increase of lateral interfluve flow velocity, and (2)

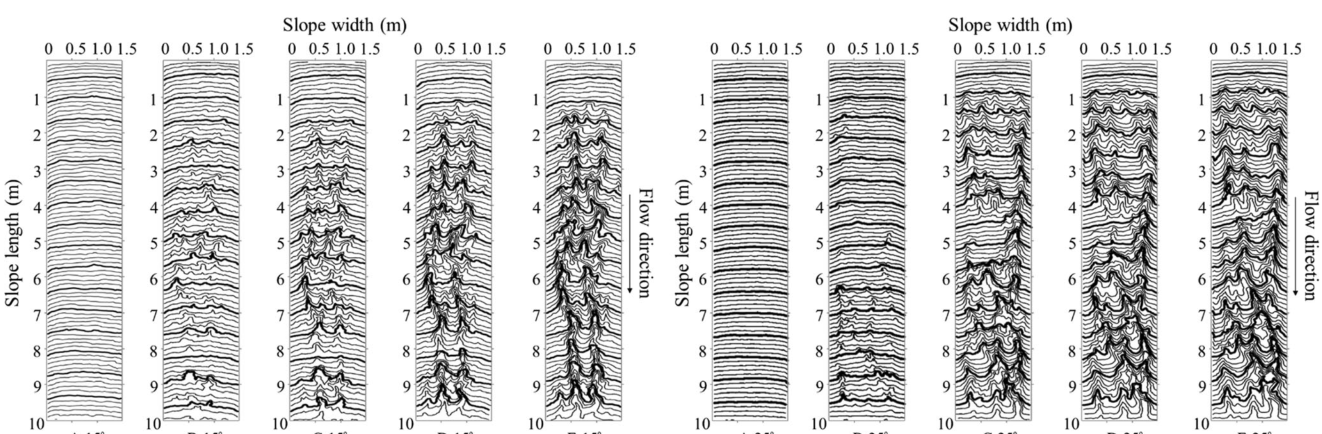

Fig. 6 Contour lines of the initial hillslope surface (A-15°, A-25°) and contour lines after the first (B-15°, B-25°), second (C-15°, C-25°), third (D-15°, D-25°), and fourth (E-15°, E-25°) rains with slope gradients of 15° and 25°

Table 3 Inter-rill, rill, and lateral interfluve flow velocities for the four successive rains

Slope gradient (°)	Successive rains	Flow velocity (cm s^{-1})		
		Inter-rill	Rill	Lateral interfluve
15	1st	21.5 ± 9.5b	24.6 ± 6.0b	12.6 ± 3.7c
	2nd	15.4 ± 4.9b	27.9 ± 7.1b	15.6 ± 4.6c
	3rd	15.3 ± 1.2b	28.7 ± 10.9b	20.5 ± 3.9b
	4th	15.3 ± 1.5c	32.3 ± 15.0b	20.6 ± 3.1b
25	1st	28.4 ± 15.0b	29.3 ± 9.7b	16.8 ± 4.7c
	2nd	20.8 ± 5.8b	31.9 ± 9.1b	20.5 ± 7.9b
	3rd	20.1 ± 6.4b	37.5 ± 15.3b	25.2 ± 5.0b
	4th	19.0 ± 2.4c	51.3 ± 17.9a	25.9 ± 4.3b

Note: a, b, and c represent turbulent flow, transition flow, and sheet flow, respectively

meander cutoffs (similar to river diversion) of rill flow on rill channel at the sharp turn (corner) enhanced with the increase of rill flow velocity. The combined result was a decrease in secondary rill length but an increase of main rill length and width (Fig. 3a, b). The above results fit well with Gómez et al. (2003), who indicate that the processes of merging unsuccessful rills into successful rills facilitate rill length and rill density decreases and eventually lead to a steady state of rill network with a minimum energy expenditure.

In another aspect, with merging of secondary rills into main rills, more overland flow concentrated in the main rill. Larger rill flow discharge and flow energy at the fourth rain resulted in scouring the rill toe. Rill flow and lateral interfluve flow both enhanced the main rill widths, which contributed to a higher possibility of rill piracy. Rill flow is the main factor that scoured the rill toe while lateral interfluve flow enhanced both rill top width and bottom width by vortex erosion adherent to rill sidewall. As a result, rill cross-section shape gradually changed from U-shape to lagena-shape (Fig. 4d). More soil clods overhung the rill bed and resulted in the probability of rill sidewall collapse increasing. Particles of rill sidewall that entrained by lateral interfluve flow and the collapsed soil blocks were two significant sediment sources to the rill channel.

3.4.2 Plow pan effects

Various impact factors comprehensively led to differences between widths of main rill and secondary rill. Rill widths before reaching the plow pan are functions of overland flow discharge and channel slope (Wells et al. 2013; Bingner et al. 2016). Secondary rill beds were not cut down to the plow pan, their widths were only affected by rill flow discharge and rill bed slope. At the same slope gradient, flow discharges were determined by contributing areas. Flow discharge of secondary rills increased first and then decreased, which led to secondary rill widths increasing fast at the second and third rains and relatively slower at the fourth rain (Fig. 3b). Secondary rill widths at the 25° slope gradient showed smaller values than those at the 15° slope gradient, which could be attributed to the negative relationship between rill width and rill bed slope gradient (Wells et al. 2013).

The dominant impact factors of main rill width were rill flow discharge, soil erodibility, and rill bed slope. Before reaching the plow pan (first, second, and third rain), main rill widths increased at a relatively low rate due to rill network development and contributing area enlargement. The plow pan played a key role during the latter two rains by restricting the rill deepening processes (Fullen 1985). Due to some parts of the main rills (mostly located at the 7.7–8.5 m slope length) being cut down to the plow pan (> 20 cm), the average bed incision rate of main rills increased slowly (3.9 and 4.4 cm for the 15° and 25° slope gradients, respectively). This led to a shoulder on the top of the plow pan for lagena-shaped rills (Fig. 4d). Some studies (Fullen 1985; Shen et al. 2015) also showed that the presence of a plow pan often revealed a shoulder at 20 to 30 cm depth. The main erosion process changed from bed incision to sidewall expansion. Rill widening accelerates as the energy of the flowing water shifts from a vertical force to a horizontal force. A bunch of equations were developed to predict channel widths by using flow discharge without taking a less erodible layer into account (Nachtergaele et al. 2002). However, significant underestimation was detected when less erodible layer (plow pan, clay inriched (Bt-) horizon, bed rock) was exposed to concentrated flow. To increase the prediction accuracy, either the equation exponents should be increased or both flow rate and slope gradient should be considered in the newly formed equations (Nachtergaele et al. 2002; Wells et al. 2013). Therefore, the data obtained in this study when both concentrated flow and lateral interfluve flow were considered does have merit in providing basic information to predict channel widths on steep hillslopes (Gordon et al. 2007).

3.4.3 Secondary headcuts impacts

Rill bed incision was determined by two sub-processes: rill flow shear incision and rill headcut incision. Rill flow shear incision is the process of soil particles of rill bed entrained by concentrated flow without forming the secondary headcut (it was determined by rill bed slope, flow velocity, width, and depth) (Bennett et al. 2000). Rill flow shear incision occurred before a headcut arrived and after a headcut moved forward. The bed incision rate was relatively low and varied between 0.08 and 0.28 cm min^{-1} (Fig. 7). The duration of this process lasted 1.1 to 2.9 times longer than secondary headcut incision. Secondary headcuts, which mostly appear at the position where there is a considerable difference in erodibility between surface and subsurface soil, make a great contribution to rill bed incision (Bryan and Poesen 1989). Mature rill networks concentrated large amounts of runoff during the third and fourth rains, and secondary headcuts in rills prompted the bed incision rate to increase fast (Fig. 1c). Failure of rill bed seals is often triggered by crack and knickpoint formation, which further facilitates headcuts advance (Bennett et al. 2000; Favis-Mortlock et al. 2000). For a certain cross section of the hillslope, rill depth increased through two processes: rill flow shear incision and rill headcut incision. The period when a headcut was detected at the cross section was defined as the headcut incision period. The remaining time was defined as the rill flow shear incision period. The bed incision rate of secondary headcut was 2–7.5 times larger than rill flow shear incision (Fig. 7). After the headcut went through a cross section, the bed incision rate varied at a relatively high level for a short period and then decreased due to the disturbed rill bed has relatively high erodibility (compared to undisturbed bed) without the protection of seals. Bryan and Poesen (1989) indicated that rill incision always arose through the formation of a knickpoint, although not all knickpoints became rills. Bennett et al. (2000) also indicated that sediment yield from

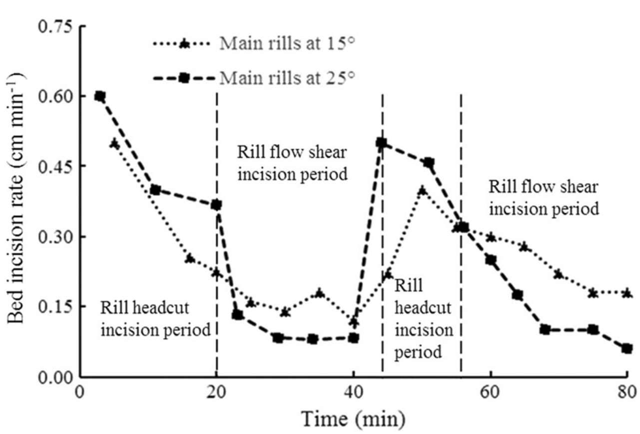

Fig. 7 General bed incision rate of main rills (selected examples from one cross section at the slope length of 5.5 m; vertical dashed lines show rill flow shear incision period and rill headcut incision period) with slope gradients of 15° and 25°

soil surface was nearly zero prior to bed incision. The results of this study verified their conclusions, while they also indicated that bed incision detachment caused by rill flow shear stress before and after headcut incision, though very slight, cannot be ignored. Rill bed incision and rill head advance are two complementary processes. The most active phase of rill bed incision always goes with the new headcut formation and advance. Initial depth of a rill equals to the initial headcut height. During the following bed incision process, rill depth increasing rate is largely determined by secondary headcuts incision process. Therefore, conservation practices should focus on preventing both initial and secondary headcut formation on hillslopes (e.g., intercepting runoff from upstream of channel head).

4 Conclusions

Four successive simulated rains that focused on rill network development and rill morphological characteristics under slope gradients of 15° and 25° were conducted. Rill network morphology was analyzed by high resolution DEMs acquired by TLS. The results showed that (1) rill erosion was the main contributor of total soil loss, both expressed as a power equation to the product of slope gradient and accumulated rainfall. (2) Rill networks evolved through an initial phase of increasing complexity and followed by a phase of stable rill network; (3) main rill length, width, depth, and degree of contour line departure increased as rainfall proceeded while secondary rill length and rill density increased and then decreased with time; and (4) rill density, average distance between two rill headcuts, degree of contour line departure increased, and initial rill head occurrence position moved upstream with the increase of slope gradient. (5) Rill headward retreat dominated the first and second rains while bed incision and sidewall expansion were the main processes at the third and fourth rains.

Over the four successive rains, rills showed relatively high lengthening, widening, and incision rates during the early periods of development. More attention should be paid to rill piracy, plow pan, and secondary headcuts when modeling rill erosion process.

Acknowledgements The authors would like to thank Dr. Glenn V. Wilson's help in revising the English grammar, as well as Dr. Robert R. Wells, the editors, and anonymous reviewers for their valuable comments and suggestions.

Funding information This study was supported by the National Natural Science Foundation of China (Grant no. 41271299 and 4171101192), Opening Funds of MWR Key Laboratory of Soil and Water Loss Process and Control in the Loess Plateau (No. 2017001), Special-Funds of Scientific Research Programs of State Key Laboratory of Soil Erosion and Dryland Farming on the Loess Plateau (A314021403-C2), and China Scholarship Council.

References

Bennett SJ, Alonso CV, Prasad SN, Römkens MJM (2000) Experiments on headcut growth and migration in concentrated flows typical of upland areas. Water Res Res 36(7):1911–1922. https://doi.org/10.1029/2000WR900067

Berger C, Schulze M, Rieke-Zapp D, Schlunegger F (2010) Rill development and soil erosion: a laboratory study of slope and rainfall intensity. Earth Surf Proc Land 35(12):1456–1467. https://doi.org/10.1002/esp.1989

Bewket W, Sterk G (2003) Assessment of soil erosion in cultivated fields using a survey methodology for rills in the Chemoga catchment. Ethiopian Agriculture Ecosystem Environment 97:81–93

Bingner RL, Wells RR, Momm HG, Rigby JR, Theurer FD (2016) Ephemeral gully channel width and erosion simulation technology. Nat Hazards 80(3):1949–1966. https://doi.org/10.1007/s11069-015-2053-7

Brunton DA, Bryan RB (2000) Rill network development and sediment budgets. Earth Surf Proc Land 25(7):783–800. https://doi.org/10.1002/1096-9837(200007)25:7<783::AID-ESP106>3.0.CO;2-W

Bryan RB, Poesen J (1989) Laboratory experiments on the influence of slope length on runoff, percolation and rill development. Earth Surf Proc Land 14(3):211–231. https://doi.org/10.1002/esp.3290140304

Favis-Mortlock DT, Boardman J, Parsons AJ, Lascelles B (2000) Emergence and erosion: a model for rill initiation and development. Hydrol Process 14(11-12):2173–2205. https://doi.org/10.1002/1099-1085(20000815/30)14:11/12<2173::AID-HYP61>3.0.CO;2-6

Foster GR, Lane LJ, Mildner WF (1983) Seasonally ephemeral cropland gully erosion. Proceedings of Natural Resources Modeling Symposium. Pingree Park, CO., USA, 16–21:463–365

Fullen MA (1985) Compaction, hydrological processes and soil erosion on loamy sands in east Shropshire, England. Soil Till Res 6(1):17–29. https://doi.org/10.1016/0167-1987(85)90003-0

Gessesse GD, Fuchs H, Mansberger R, Klik A, Rieke-Zapp DH (2010) Assessment of erosion, deposition and rill development on irregular soil surfaces using close range digital photogrammetry. Photogramm Rec 25(131):299–318. https://doi.org/10.1111/j.1477-9730.2010.00588.x

Giménez R, Govers G (2001) Interaction between bed roughness and flow hydraulics in eroding rills. Water Resour Res 37(3):791–799. https://doi.org/10.1029/2000WR900252

Gómez JA, Darboux F, Nearing MA (2003) Development and evolution of rill networks under simulated rainfall. Water Resour Res 39(6):1148

Gong JG, Jia YW, Zhou ZH, Wang Y, Wang WL, Peng H (2011) An experimental study on dynamic processes of ephemeral gully erosion in loess landscape. Geomorphology 125(1):203–213. https://doi.org/10.1016/j.geomorph.2010.09.016

Gordon LM, Bennett SJ, Bingner RL, Theurer FD, Alonso CV (2007) Simulating ephemeral gully erosion in AnnAGNPS. Trans ASABE 50(3):857–866. 10.13031/2013.23150

Govindaraju RS, Kavvas ML (1994) A spectral approach for analyzing the rill structure over hillslopes. Part 1. Development of stochastic theory. J Hydrol 158(3-4):333–347. https://doi.org/10.1016/0022-1694(94)90061-2

Gravelius H (1914) Flusskunde. Goschen'sche Verlagshandlung, Berlin, p 176

He J, Li X, Jia L, Gong H, Cai Q (2014) Experimental study of rill evolution processes and relationships between runoff and erosion on clay loam and loess. Soil Sci Soc Am J 78(5):1716–1725. https://doi.org/10.2136/sssaj2014.02.0063

Hofer M, Lehmann P, Stähli M, Seifert S, Krafczyk M (2012) Two approaches to modeling the initiation and development of rills in a man-made catchment. Water Resour Res 48:1–17

Horton RE (1945) Erosional development of streams and their drainage basins. Hydrophysical approach to quantitative morphology. Bull Geol Soc Am 56(3):275–370. https://doi.org/10.1130/0016-7606(1945)56[275:EDOSAT]2.0.CO;2

Lal R (2002) Gully erosion. Encyclopedia of soil science. Marcel Dekker, New York, pp 630–632

Li G, Abrahams AD, Atkinson JF (1996) Correction factors in the determination of mean velocity of overland flow. Earth Surf Proc Land 21(6):509–515. https://doi.org/10.1002/(SICI)1096-9837(199606)21:6<509::AID-ESP613>3.0.CO;2-Z

Liu BY, Nearing MA, Risse LM (1994) Slope gradient effect on soil loss for steep slopes. Trans ASAE 37(6):1835–1840. 10.13031/2013.28273

Mancilla GA, Chen S, McCool DK (2005) Rill density prediction and flow velocity distributions on agricultural areas in the Pacific Northwest. Soil Till Res 84(1):54–66. https://doi.org/10.1016/j.still.2004.10.002

Momm HG, Wells RR, Bennett SJ, Gilley A (2016) Image analysis for quantifying spatiotemporal evolution of rill networks in laboratory experiments. In: Garcia and Hanes (eds) Proceedings of the River-Flow 2016—Eighth International Conference on Fluvial Hydraulics; Constantinescu. Taylor & Francis Group, St. Louis, MO, U.S.A., July 12–15, 2016

Nachtergaele J, Poesen J, Sidorchuk A, Torru D (2002) Prediction of concentrated flow width in ephemeral gully channels. Hydrol Process 16(10):1935–1953. https://doi.org/10.1002/hyp.392

Shen H, Zheng F, Wen L, Lu J, Jiang Y (2015) An experimental study of rill erosion and morphology. Geomorphology 231:193–201. https://doi.org/10.1016/j.geomorph.2014.11.029

USDA NRCS (1999) Soil taxonomy: a basic system of soil classification for making and interpreting soil surveys. Agric. Handbook 436, 2nd edn. U.S. Government Printing Office, Washington, DC

Vinci A, Brigante R, Todisco F, Mannocchi F, Radicioni F (2015) Measuring rill erosion by laser scanning. Catena 124:97–108. https://doi.org/10.1016/j.catena.2014.09.003

Wells RR, Bennett SJ, Alonso CV (2010) Modulation of headcut soil erosion in rills due to upstream sediment loads. Water Resour Res 46(12):1–16

Wells RR, Momm HG, Rigby JR, Bennett SJ, Bingner RL, Dabney SM (2013) An empirical investigation of gully widening rates in upland concentrated flows. Catena 101:114–121. https://doi.org/10.1016/j.catena.2012.10.004

Wells RR, Momm HG, Bennett SJ, Gesch KR, Dabney SM, Cruse R, Wilson GV (2016) A measurement method for rill and ephemeral gully erosion assessments. Soil Sci Soc Am J 80(1):203–214. https://doi.org/10.2136/sssaj2015.09.0320

Wu Q, Wang L, Wu F (2014) Tillage—impact on infiltration of the loess plateau of China. Acta Agri Scandi, Section B—Soil Plant Sci 64(4):341–349

Yang M, Tian J, Liu P (2006) Investigating the spatial distribution of soil erosion and deposition in a small catchment on the loess plateau of China, using 137Cs. Soil Tilla Res 87(2):186–193. https://doi.org/10.1016/j.still.2005.03.010

Zhang HX (1983) The characteristics of hard rain and its distribution over the loess plateau. Acta Geograph Sin 38(4):416–425 (in Chinese with English Abstract)

Zheng FL, Tang KL (1997) Rill erosion process on steep slope land of the loess plateau. J Sediment Res 12(1):52–59

Zhou PH, Wang ZL (1987) Soil erosion rainfall standard in the loess plateau. Bull Soil Water Conserv 7(1):38–44 (in Chinese with English Abstract)

Zhou PH, Zhang XD, Tang KL (2000) Rainfall installation of simulated soil erosion experiment hall of the State Key Laboratory of Soil Erosion and Dryland Farming on Loess Plateau. Bull Soil Water Conserv 20(4):27–30 **45** (in Chinese with English Abstract)

Zhu XM (1956) Soil erosion classification at the loessial region. Acta Pedol Sin 4(2):99–116 (in Chinese)